



ORIGINAL ARTICLE

2D ceramic grains images manipulations: A simple geometrical characterization and grain domain recreation algorithm



Filipe L. Braga

Instituto Federal de Educação, Ciências e Tecnologia do Espírito Santo, Campus Cariacica, Cariacica, ES, Brazil

ARTICLE INFO

Article history:

Received 14 March 2017

Revised 29 June 2017

Accepted 30 June 2017

Available online 6 July 2017

Keywords:

Ceramic grains

Voronoi diagrams

Geometrical characterization

Lattice creation algorithm

ABSTRACT

The precision and accuracy of certain simulations in nanoscience, fluid dynamics and biotechnology in the analyses of boundary conditions problems with real experimental results are in general related to the characteristics of numerical approach used and subsequently to the morphological structure of lattices used along these calculations. The more the lattice used approximates to the original boundary or initial condition problem more precise the simulation would be. This work shows a simple algorithm that can be used to build huge lattices containing the main geometrical structures statistically similar to experimental 2D image data of ceramic grains by using some freeware software.

© 2017 The Author. Production and hosting by Elsevier B.V. on behalf of King Saud University. This is an open access article under the CC BY-NC-ND license (<http://creativecommons.org/licenses/by-nc-nd/4.0/>).

1. Introduction

In the area of nano-science, biotechnology, fluid dynamics and other scientific research branches the investigation of the main characteristics or nature of the interactions on each system can be developed by means of computational simulations [1–7]. In general, these approaches involve the solution of partial differential equations or ordinary differential equations and a big amount of these set of equations are boundary value problems.

Particularly, the matching between solution of the Dirichlet and Neumann boundary condition problems that emerge on these analyses and the real system are strictly correlated to the right choose of the lattice used to solve the differential equations [8–11].

Besides the numerical solution of differential equations there are the stochastic models [12], classical molecular dynamics simulations [13] and the cellular automata modeling [14,15] that are strongly dependent on the lattice used to role the simulations. Hence, the determination of geometrical structures of these lattices are very important for the correct accuracy of the models investigated.

One of the branches in applied physics research that requires the accurate description of the lattice is the analyses of superconductors junctions [16,17]. At these theoretical studies, part of them developed using percolation theory [18–20], the similarity between real grains morphology and the simulated ones are suitable important. For example, the area of the grains and the linear size of a junction can determine the behaviour of the current density associated with the Cooper pairs [21–23].

The present article develops an algorithm based on freeware software capable of characterize qualitatively the distributions of area and linear length of a grain edge per site of a scanned electronic microscopy image of a ceramic material containing the grains edges. Consequently, with all the statistical information obtained a modified Voronoi diagram algorithm is proposed to reconstruct the original grain image with great similarity and determine exactly the connectivity of the grains.

2. Thecnique and results

The algorithm here proposed here is similiar to the one developed by Tuan et al. [24], and is useful to deal with any kind of source image, otherwise, a scanned electronic microscopy image have a gray scale pattern of colors. Due to the quality of the original image used at the example here shown, modifications on the color contrast was performed in order to clarify the grain edges and the resulting image is represented in Fig. 1. This previous processing of the image can be performed using any manipulation software, here GIMP [25] was used.

E-mail address: filipe.braga@ifes.edu.br

Peer review under responsibility of King Saud University.



Production and hosting by Elsevier

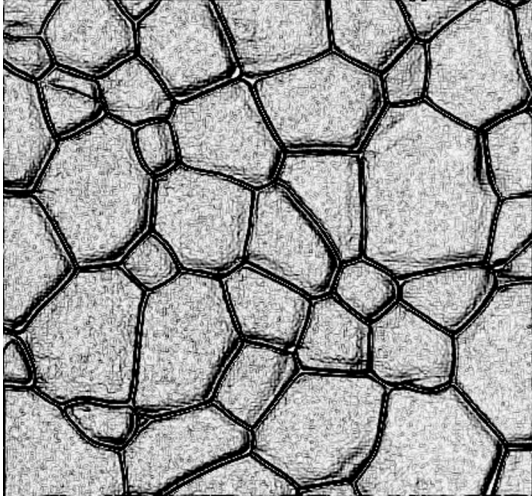


Fig. 1. Processed image is in gray scale format the original doped TiO_2 SnO_2 based electronic ceramics micrography using GIMP v.2.8. The original image is the Fig. 6 of Ref. [26].

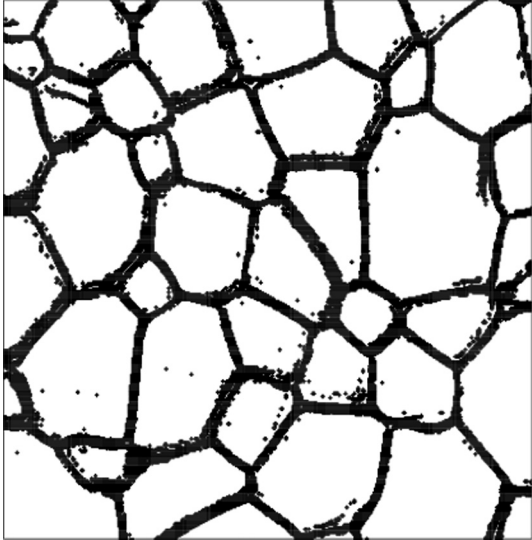


Fig. 2. The black dots represents the pixels associated with specific black color.

In order to scan the ceramic image the software *ImageMagick* [27] was used to convert the *jpeg* image file into a *.txt* file. The output file obtained is a text file that contains the pixels coordinates as integer numbers and the color associated with each pixel described by a *srgb* color code presented in three formats being one of them the corresponding hexadecimal format code for each kind of color.

The next step of the technique is a clean-up procedure. The pixels coordinates (i, j) and the hexadecimal color code must be selected from the original text file, and all other symbols and information removed. Now, is possible to scan the image inside in an array \mathbf{A} of integer numbers and associate a number to each color code.

The most important color at this array is black because it was the color associated with the ceramic grains edges. From the point of view of array elements, we create a 2-D vector of integer values called $\mathbf{A}_{n,m}$ with 0 to black pixels and 1 for all other kinds of colors. Here, m, n are the size in pixels of the original picture ($n \times m$) and represent the dimensions of the vector \mathbf{A} . Computing only the black pixels the result obtained from the processing of Fig. 1 is shown in Fig. 2.



Fig. 3. Dendritic formation near the ceramic grain edge that can generate some virtual labels associated with the determination of element label. Black box represents the grain edge and other color represents the grains areas.

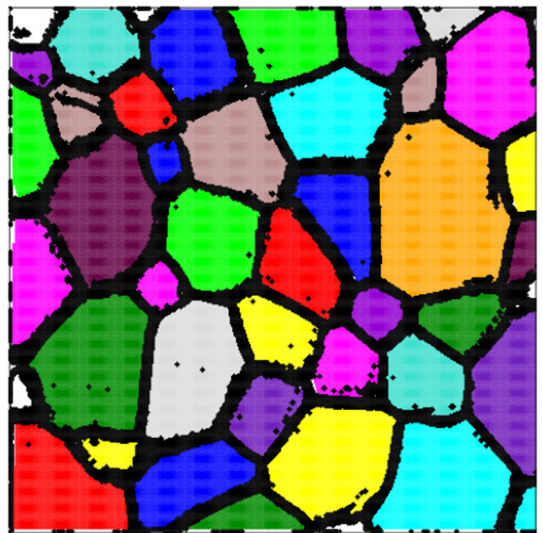


Fig. 4. Determination of each grain associating to them a unique label, for the picture of Fig. 3. Each color is related to a specific grain/label.

As observed some pixels inside the ceramic grains are black, due to the inhomogeneity of the original image. To remove part of these black pixels that do not belong to grain edges, a line search across the array considering it as a rectangular regular lattice was performed a couple of times. Along the search, each black element \mathbf{A}_{ij} surrounded by more than 3 white first nearest neighbors was changed from 0 to 1. Given the huge number of pixels determining each grain edge, the boundary of the grains was not affected by this process.

The most difficult step was to determine the region/area of the array \mathbf{A} that belongs to each ceramic grain. To perform it, the array \mathbf{A} containing only two kinds of elements 0 and 1 was scanned, going from line 1 up to m and from column 1 up to n . Every time that the forward element $\mathbf{A}_{ij+1} \neq 0$ and the instant element $\mathbf{A}_{ij} \neq 0$ or 1, then the operation $\mathbf{A}_{ij+1} = \mathbf{A}_{ij}$ was evaluated. Doing that, if $\mathbf{A}_{ij+1} \neq 0$ or 1 but $\mathbf{A}_{ij} = 0$ then $\mathbf{A}_{ij+1} = k$ where k is an integer number and is the label associated with the grain where the proposed pixel belongs. The determination of k must be done

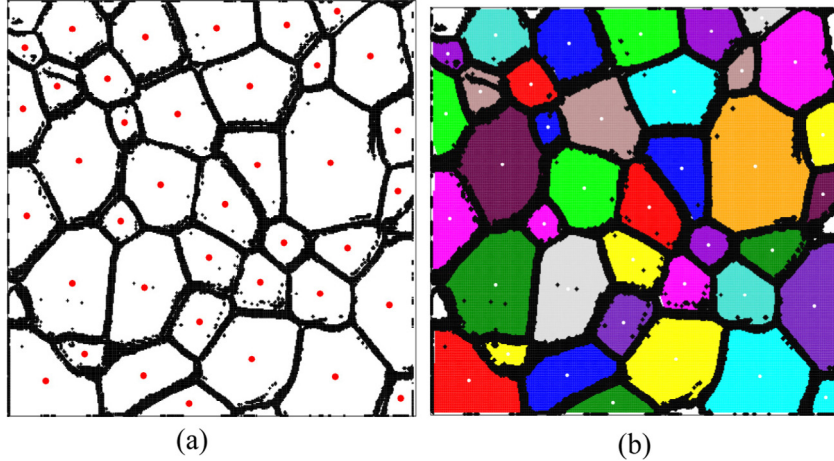


Fig. 5. (a) Picture with the red dots representing the centroid of each grain and the black dots representing the grain edge. (b) Picture with the white dots representing the centroid of each grain.

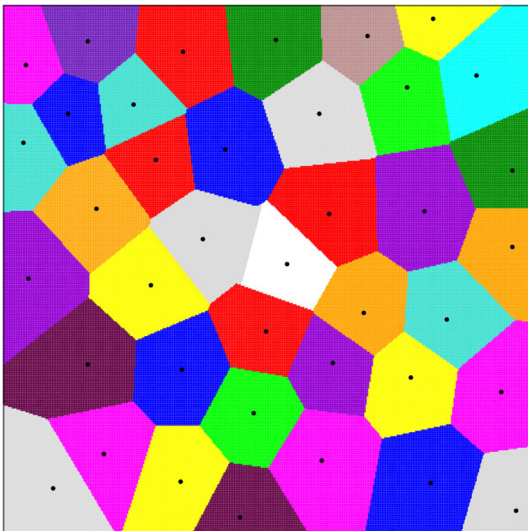


Fig. 6. Voronoi diagram built by using the centroid indexes (\bar{i}_l, \bar{j}_l) associated with the original ceramic. The black dots represent the centroid of each grain/Voronoi cell.

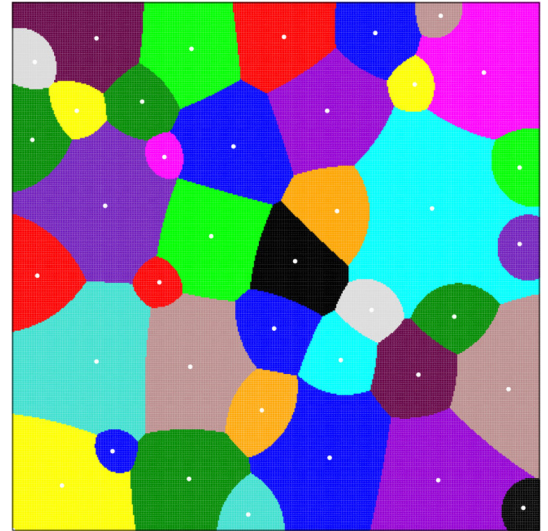


Fig. 7. Voronoi like diagram built by using the centroid indexes (\bar{i}_l, \bar{j}_l) associated with the original ceramic, and a weight factor w_l associated with each site l . The white dots represent the centroid of each grain/Voronoi like cell.

partially looking all nearest neighbors of element A_{ij+1} and by analyzing the storage array \mathbf{G} (initially $G_i = 0$) associated with the labels of all the detected ceramic grains. If there is some element around $A_{ij+1} \neq 0$, or 1 then k must be the label associated with this non-zero element. On the other hand, if every element are equal to 0 or 1, then k must be the smallest i index of the zero elements of array \mathbf{G} , and every time that search across \mathbf{G} occur the element G_i receive the correspondent index $G_i = i$ becoming a non-zero element.

At the end of this scanning process, the array \mathbf{A} has labels $0, 1, \dots, M$. Unfortunately, some labels explicitly split some grains because of some dendritic formation of the grains edge similar to the one presented in Fig. 3.

Generally, M was bigger than the real number of ceramic grains. In order to reduce M for the real number of grains $M_r - 1$, firstly the number of elements of \mathbf{A} with each label was determined, then another line search through \mathbf{A} was performed and every time that the first neighbours of A_{ij} had more than two distinct labels (not considering 1 or 0) the label of the smaller group was changed by the label of the biggest group. The result obtained after this procedure, for the picture of Fig. 2 is shown in Fig. 4.

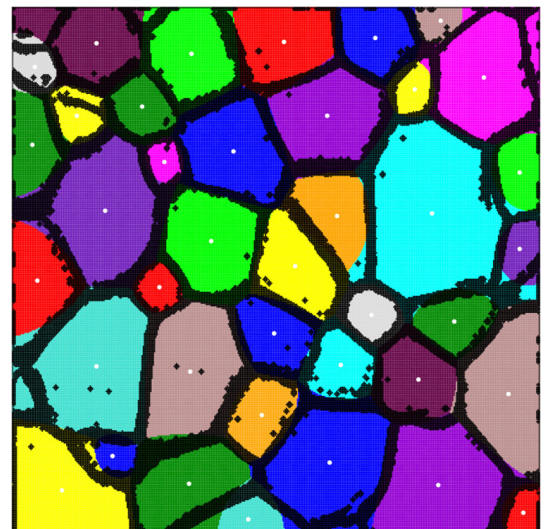


Fig. 8. Superposition of Fig. 7 (diagram built by the proposed Voronoi like algorithm) by Fig. 5(a) (original diagram cells edges).

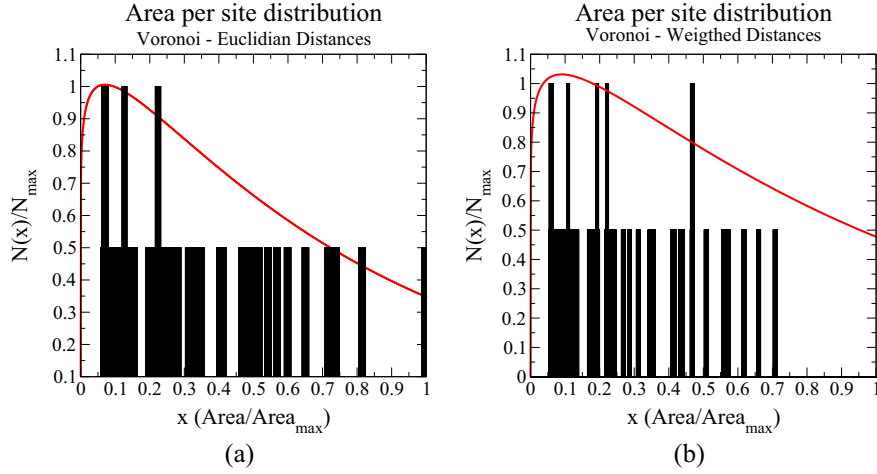


Fig. 9. Histogram associated with the normalized number of sites per area, (a) for typical Voronoi diagram and (b) for the original ceramic produced by the algorithm. The red curves are the non-linear fit for distributions, for (a) $N(x)/N_{\max} = 1.45(x)^{0.1} \exp(-x/0.7)$ and (b) $N(x)/N_{\max} = 1.45(x)^{0.1} \exp(-x/0.9)$.

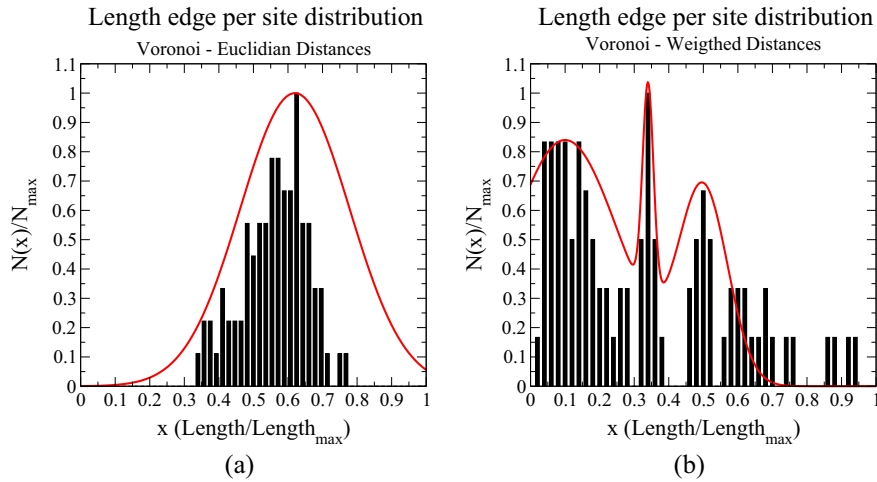


Fig. 10. Histogram associated with the normalized number of sites per edge length, (a) for typical Voronoi diagram and (b) for the original ceramic produced by the algorithm proposed. The red curves are the non linear fit of the histograms for (a) $N(x)/N_{\max} = \exp(-20(x - 0.62)^2)$ and (b) $N(x)/N_{\max} = 0.5[1.4e^{-50(x-0.21)^2} + 2e^{-64(x-0.6)^2} + e^{-1700(x-0.42)^2}]$.

At this stage of the algorithm, the array \mathbf{A} has values 0, for the grains edges and values $(2, \dots, M_r)$ for the elements belonging to the grains. The area of a grain l was determined as the total number of elements $\mathbf{A}_{i,j} = l$. In order to determine the edge length between two grains another line search through \mathbf{A} was performed, going from line $i = 1$ to n and column $j = 1$ up to m . During this line search an auxiliary array \mathbf{L} was used and the element $L_{p,k}$ stored the number of elements $\mathbf{A}_{i,j}$ at the edge between grains p and k ($2 < p, k < M_r$ and initially $\mathbf{L} = 0$). Along the line search the values of $\mathbf{A}_{i,j}$ were stored in variables $v_{1,2,3}$, representing the actual element read v_1 , and the two predecessors read elements $v_{2,3}$. Every time that $v_1 = 0$, a grain edge is reached, so the value v_2 is the label of the grain original analyzing, so it was saved in variable p . After this edge-event, the line search continues, but the values of the labels of $\mathbf{A}_{i,j}$ were stored at variable v_3 , and when $v_3 \neq 0, k = v_3$ was set, determining the other grain participating in the edge. Hence, element $L_{p,k}$ was updated with a unit. At the end of the line search only the elements $L_{pk} \neq 0$ indicates the connectivity (first neighbors) for all grains and consequently the size of the edge between grains $\{p, k\}$.

Knowing the label of each pixel, is possible to determine the centroid of each ceramic grain, by calculating the media indexes (\bar{i}_l, \bar{j}_l) , associated with label l by computing the equations

$$\bar{i}_l = \frac{1}{q} \sum_{s=1}^q i_{ls}, \quad (1)$$

$$\bar{j}_l = \frac{1}{q} \sum_{s=1}^q j_{ls}, \quad (2)$$

where q is the total number of pixels with label l . Plotting the grain edges and the grain picture is possible to clearly visualize these media indexes as shown in Fig. 5.

In order to determine the morphology of a Voronoi diagram [28] built using the same rectangular regular lattice \mathbf{Vor} with $n \times m$ elements and the centroids of the original ceramic the region of influence of each centroid was determined calculating the euclidian distance d_l between the element \mathbf{Vor}_{ij} and the indexes (\bar{i}_l, \bar{j}_l) as

$$d_l = \sqrt{(i - \bar{i}_l)^2 + (j - \bar{j}_l)^2} \quad (3)$$

if d_l is minimum, when compared to all the centroids, then the element \mathbf{Vor}_{ij} receive the label l and is part of the corresponding Voronoi diagram cell. A typical Voronoi Diagram obtained for the centroids of the analysed ceramic can be observed in Fig. 6.

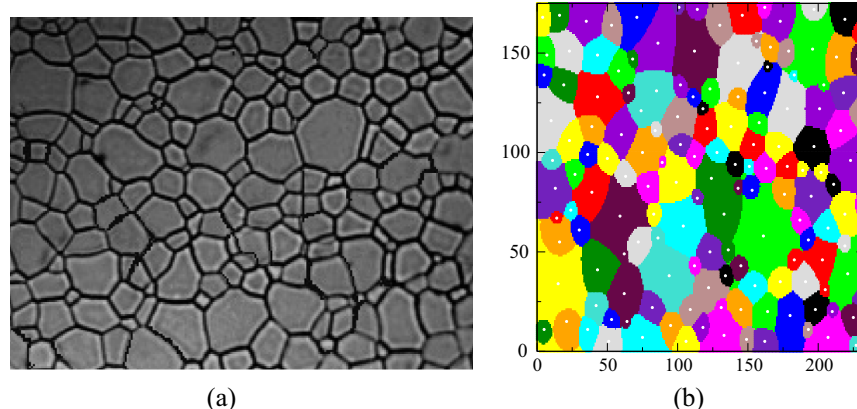


Fig. 11. (a) The modified image of the experimental ceramical microstructure of the polycrystalline UO₂ pellet from Ref. [31]. (b) reconstructed Voronoi diagram build using the procedure described before.

Comparing Figs. 6 and 5(b) is possible to observe that geometrically the number of large sites (sites with more than 6% of the total area of the image¹) and small sites (sites with less than 2% of the total image area) are not matching each other.

In order to reproduce the same behavior of the original ceramic was proposed to build a new diagram based on the Voronoi algorithm, but instead of calculating the euclidean distance between two elements of **Vor** a weight factor w_l was introduced at the calculation of de distance d_l as

$$d'_l = \frac{1}{w_l} \sqrt{(i - \bar{i}_l)^2 + (j - \bar{j}_l)^2} \quad (4)$$

with w_l been the number of pixels associated with site l . On other words, it was related to the original area of the ceramic grain. This weight factor can be interpreted as a form to compute the non-linear influence of each grain at the ceramic processing manufacturing.

The result obtained by this algorithm can be observed on Fig. 7. Coupling the diagram of Fig. 7 and the original contours associated with each site as depicted in Fig. 8, is possible to observe that the proposed weight factor imposes an agreement between the original ceramic geometrical features and the built one.

In order to quantitatively compare the results obtained for the original ceramic and the typical Voronoi Diagram using the centroids of each grain previously determined the normalized histograms for the number of sites as a function of the site's area was calculated, as shown in Fig. 9(a) and (b), where a distribution function can be casted in format of a gamma functions as proposed.

At the same way the normalized histograms for the number of sites per edge length, presented a continuous behaviour of gaussian functions, as observed on Figs. 10 (a) and (b).

These calculations related to the distribution of areas and lengths of edges for the grains, can be used as a source probability distribution function (p.d.f.) to build a large diagram that recover the same statistical behaviour of the original ceramic. To evaluate this one may use some Markov chain Monte Carlo algorithm as Metropolis-Hastings [29], in order to determine the weight factor (area related) for each Voronoi like diagram cell, and at indirectly determine the position center of each grain cell.

A procedure that evaluate the proposed mechanism to determine large diagramns, can be depicted as the following five step algorithm:

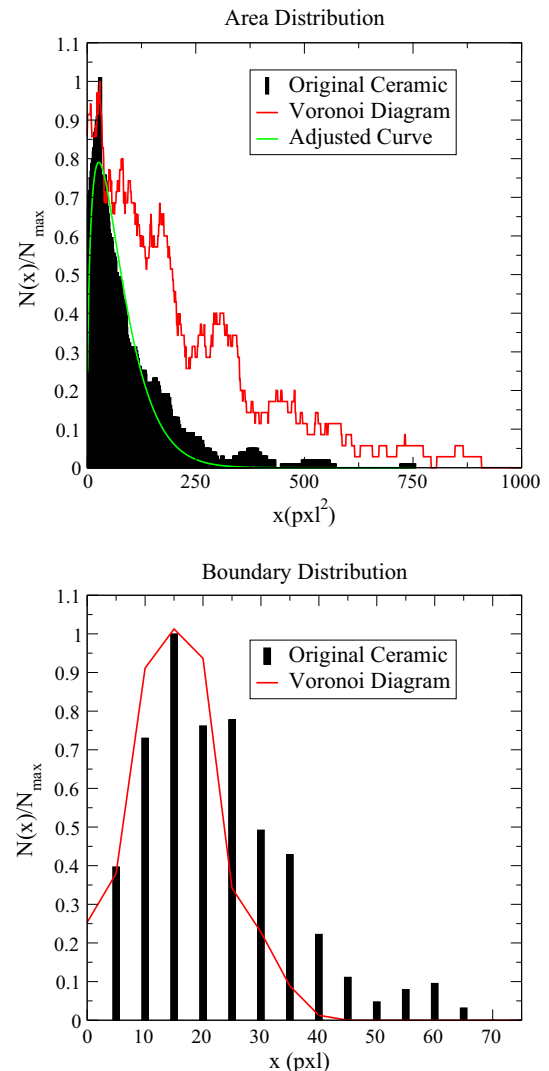


Fig. 12. Correspondent distribution functions for the area and the boundary length, for the original experimental ceramic image, and for the correspondent Voronoi diagram. The green line represents the adjusted curve associated with the area of the experimental microstructure image. the associated function is $N(x)/N_{\max} = A_0 \cdot \sqrt{x} \exp [A_1 \cdot (x - A_2)^2]$, been $A_0 = 481.32, A_1 = -1.0855 \times 10^{-5}$ and $A_2 = -834.47$.

¹ Calculated in termos of pixels.

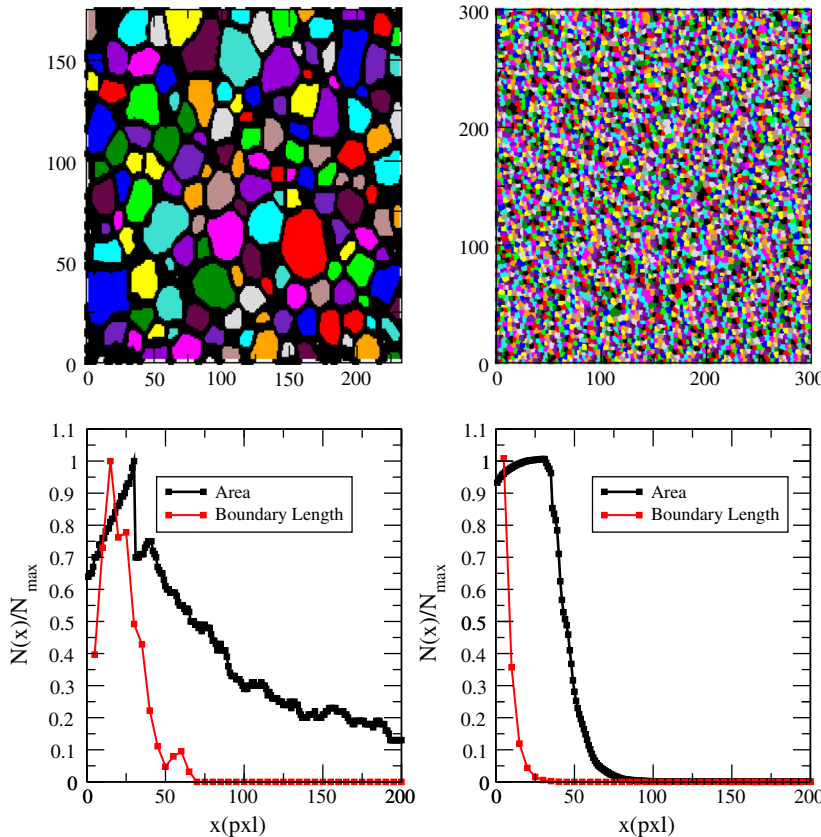


Fig. 13. Statistical comparision between the original lattice produced based on the original ceramic microstructure of UO_2 from Fig. 1 of Ref. [31] (lattice with $N_s = 171$ sites), and the correspondent Voronoi diagram (Voronoi lattice) with $N_s = 10^4$ sites.

1. Determine the areas A_s of N_s sites using the p.d.f. function for the areas, via Metropolis-Hastings algorithm.
2. Determine approximately the center position of the N_s sites, on a similar way as proposed for the construction of the Voronoi Diagram.
3. Determine the area of influence of each Voronoi Cell.

The third step can be held on the same one way as depicted before. The second step can be determined by using an auxiliar square lattice of specific length L , where the N_s sites, topologically considered as spheres of radius r_s ,² associated with the area A_s must be set up covering the square lattice on a way to minimize the vacancies between each one of the N_s sites, on a similar procedure as proposed in the rearrangement of containers as proposed in Ref. [30].

In order to validate the previous algorithm for the characterization of ceramic samples, we analyze the main features of the uran dioxide (UO_2) polycrystalline pellet image collected on Fig. 1 of Ref. [31]. The reconstructed image, the correspondent Voronoi Diagram and the centers of each grain can be observed can be observed at Fig. 11.

The distribution functions associated with experimental microstructure and the corresponding Voronoi diagram are shown in Fig. 12.

Using the proposed curve $N(x)/N_{\max}$ for the areas, we determine the radius of $N_s = 10^4$ sites, and determine, and using the three step procedure described we determine a huge lattice compared to the original lattice, produced with the experimental image, with

a very similar statistical feature for the area and the cells boundary length as observed in Fig. 13.

Probably, due to the stochastic behaviour of Metropolis-Hastings algorithm, the approximation of the centers of the grains/Voronoi cells, addicted to the small number of grains/sites of the originals samples, the p.d.f.'s associated with the area and the boundary length of each grain for the bigger lattice, do not exactly match the original functions. But the main goal of the proposed algorithm is achieve, with the procedure proposed we are now able to create more realistic approximated lattices, that are intrinsically correlated to experimental data.

In other words, a better computational/mathematical background to create useful random lattices that are the aim of interest to develop studies related to percolation, partial differential equations, and other sets of computational areas of interest to material science, can be performed using the proposed algorithm.

3. Conclusions

The proposed scanning algorithm is a very useful technique to manipulate 2D ceramic images containing the grains edges. A quantitative characterization of the grains edge length and area can be casted in the format of normalized histograms and the connectivity of the grains (first neighbours) can be explicitly determined. The previous features described allows the construction of huge inhomogeneous lattices statistically correlated to real ceramics, creating a useful framework for many material science research areas using a Voronoi like diagram algorithm where the influence of each grain is modulated as a weight factor related to the grain area.

² Given the square symmetry of the lattice a typical sphere with radius r can be interpreted as a box of size $2 \cdot r$.

References

- [1] D. Srivastava, M. Menon, K. Cho, Computational nanotechnology with carbon nanotubes and fullerenes, *Comput. Sci. Eng.* 3 (42) (2001).
- [2] G. Klimeck, M. McLennan, S.P. Brophy, G.B. Adams, M.S. Lundstrom, Advancing education and research in nanotechnology, *Comput. Sci. Eng.* 10 (17) (2008).
- [3] L.G. Silva, A.M.J.C. Neto, L. Gaffo, R.S. Borges, T.C. Ramalho, N. Machado, Molecular dynamics of film formation of metal tetrasulfonated phthalocyanine and poly amidoamine dendrimers, *J. Nanomater.* 2013 (2013).
- [4] Z.G. Mills, W. Mao, A. Alexeev, Mesoscale modeling: solving complex flows in biology and biotechnology, *Trends Biotechnol.* 31 (7) (2013).
- [5] A. Korobenko, M.-C. Hsu, I. Akkerman, J. Tippmann, Y. Bazilevs, Structural mechanics modeling and FSI simulation of wind turbines, *Math. Mod. Meth. Appl. Sci.* 23 (249) (2013).
- [6] M. Ghadiri, M. G Darehnaei, S. Sabbaghian, S. Shirazian, Computational simulation for transport of priority organic pollutants through nanoporous membranes, *Chem. Eng. Technol.* 36 (3) (2013).
- [7] Simone Falco, Jiawei Jiang, Francesco De Cola, Nik Petrinic, Generation of 3d polycrystalline microstructures with a conditioned laguerre-voronoi tessellation technique, *Comput. Mater. Sci.* 136 (2017) 20–28.
- [8] M. Lüscher, Properties and uses of the Wilson flow in lattice QCD, *J. High Energy Phys.* 08 (71) (2010).
- [9] F.Y. Kuo, C. Schwab, I.S. Sloan, Quasi-Monte Carlo finite element methods for a class of elliptic partial differential equations with random coefficients, *SIAM J. Numer. Anal.* 6 (50) (2012).
- [10] Dong Wang, Jun Zhao, Chao Xue, Yan Cao, Finite element simulation of vickers micro-indentation test of micro-nano-composite ceramic tool materials based on microstructure model, *Int. J. Refract. Met. Hard Mater.* 58 (2016) 34–41.
- [11] Zhiyong Wang, Peifeng Li, Voronoi cell finite element modelling of the intergranular fracture mechanism in polycrystalline alumina, *Ceram. Int.* 43 (9) (2017) 6967–6975.
- [12] O.E. Garcia, Stochastic modeling of intermittent scrape-off layer plasma fluctuations, *Phys. Rev. Lett.* 108 (2012).
- [13] T.R. Mattsson, J.M.D. Lane, K.R. Cochrane, M.P. Desjarlais, A.P. Thompson, F. Pierce, G.S. Grest, First-principles and classical molecular dynamics simulation of shocked polymers, *Phys. Rev. B* 81 (2010).
- [14] R.M. Amorim, R.S. Campos, M. Lobosco, C. Jacob, R.W. Santos, An electro-mechanical cardiac simulator based on cellular automata and mass-spring models, *Lect. Notes Comput. Sci.* 7495 (2012).
- [15] J.L. Schiff, *Cellular Automata: A Discrete View of the World*, John Wiley and Sons, 2011.
- [16] L.P. Rokhinson, X. Liu, J.K. Furdyna, The fractional A.C. Josephson effect in a semiconductor–superconductor nanowire as a signature of Majorana particles, *Nat. Phys.* 8 (2012).
- [17] P. San-Jose, E. Prada, R. Aguado, AC Josephson effect in finite-length nanowire junctions with Majorana modes, *Phys. Rev. Lett.* 108 (2012).
- [18] G. Deutscher, K.A. Müller, Origin of superconductive glassy state and extrinsic critical currents in high-Tc oxides, *Phys. Rev. Lett.* 59 (1745) (1987).
- [19] G. Bianconi, Superconductor-insulator transition in a network of 2d percolation clusters, *Euro Phys. Lett.* 101 (26003) (2013).
- [20] Abbas Ali Saberi, Recent advances in percolation theory and its applications, *Phys. Reports* 578 (2015) 1–32, Recent advances in percolation theory and its applications.
- [21] Y. Hirata, K.M. Kojima, M. Ishikado, S. Uchida, A. Iyo, H. Eisaki, S. Tajima, Correlation between the interlayer Josephson coupling strength and an enhanced superconducting transition temperature of multilayer cuprate superconductors, *Phys. Rev. B* 85 (2012).
- [22] K.G. Fedorov, M.V. Fistul, A.V. Ustinov, Pinning of charge and flux solitons in disordered Josephson junction arrays, *Phys. Rev. B* 84 (2011).
- [23] P. Sunwong, J.S. Higgins, Y. Tsui, M.J. Raine, D.P. Hampshire, The critical current density of grain boundary channels in polycrystalline HTS and LTS superconductors in magnetic fields, *Supercond. Sci. Tech.* 26 (2013).
- [24] Dang Anh Tuan, Vo Thanh Tung, et al., Analyzing 2d structure images of piezoelectric ceramics using imagej, *Int. J. Mater. Chem.* 4 (4) (2014) 88–91.
- [25] <http://www.gimp.org/> visited on june 28th of 2017.
- [26] M.R. Cassia-Santos, V.C. Sousa, M.M. Oliveira, P.R. Bueno, W.K. Bacelar, M.O. Orlandi, C.M. Barrado, J.W. Gomes, E. Longo, E.R. Leite, J.A. Varela, SnO₂ and TiO₂ based electronic ceramics, *Cerâmica* 47 (303) (2001).
- [27] <http://www.imagemagick.org/script/index.php> visited on june 28th of 2017.
- [28] A. Okabe, B. Boots, K. Sugihara, S.N. Chiu, *Spatial Tessellations: Concepts and Applications of Voronoi Diagrams* (Wiley Series in Probability and Statistics), John Wiley and Sons, 2000.
- [29] B.A. Berg, *Introduction to Markov Chain Monte Carlo Simulations and Their Statistical Analysis*, World Scientific, 2004.
- [30] Sheng Liu, Wei Tan, Zhiyuan Xu, Xiwei Liu, A tree search algorithm for the container loading problem, *Comput. Indust. Eng.* 75 (2014) 20–30.
- [31] W.B. Ferraz, A.C.S. Sabioni, Diffusion of gadolinium in the UO₂ nuclear fuel, *Cerâmica* 52 (2006) 143–148, 09.